Proceedings of the 1999 U.S DOE Hydrogen Program Review
NREL/CP-570-26938

MODELING OF THE SUPERCRITICAL WATER PYROLYSIS PROCESS

Robert J. Divilio
Combustion Systems Inc.
10015 Brookmoor drive
Silver Spring, MD 20901

Abstract

A high-pressure gas clean-up process has been developed to produce pure hydrogen from the product stream of the supercritical water pyrolysis of biomass. This process takes advantage of the high pressures utilized in the SCW pyrolysis process to scrub carbon dioxide from the product stream with pressurized water. The process eliminates the need to compress gasses, as only incompressible liquids are pressurized.

A model has been developed to predict the formation of char at the entrance of the SCW pyrolysis reactor. The char formation is found to occur at temperatures below the pseudo critical temperature of the water. Fast heating rates were found to decrease the amount of char that would form. However, some char formation will always occur.

A mass transfer model was developed for the water-gas shift reaction. This model was found to predict the conversion of carbon monoxide better than a model based on the bulk concentrations of CO. The model also predicts the reversible nature of the water-gas shift reaction.

A global model of the supercritical water pyrolysis process has been developed. This model tracks the reactants as they are heated from room temperature up to the reactor temperatures. The model was calibrated using the glucose pyrolysis data of Holgate, et. al. (1995) and was found to do a reasonable job of predicting Holgate's data. The model predicts the effects of heating rate and reactor temperature on the pyrolysis products.

Introduction

The Department of Energy is currently funding a research project at the University of Hawaii to produce hydrogen gas from high-moisture-content biomass using supercritical water. This work has shown that it is possible to completely gasify a paste composed of water containing 3 to 5% corn starch and 5 to 10% sawdust at supercritical conditions in a flow reactor, when an activated carbon catalyst is present. Combustion Systems Inc. (CSI) has been contracted by the National Renewable Energy Laboratory (NREL) to develop a comprehensive model of this supercritical gasification process for the Department of Energy under Subcontract Number AXE-8-17103-01. This paper summarizes the status of the first year of work on this project.

During this time period, a comprehensive heat transfer model has been developed to calculate the temperature profiles in the University of Hawaii's reactor. CSI also performed a literature review to identify the major reaction pathways for the pyrolysis of biomass in supercritical water. This work was reported in Divilio (1998). In addition to these tasks, CSI also developed a model for a high-pressure gas clean-up process that utilized the pressure of the SCW process to purify the hydrogen gas without the need for gas compression. We also developed a global model for the supercritical water pyrolysis of glucose. In developing the global model, we also developed a model that predicts the formation of char at the entrance of the reactor and a mass transfer model for the water-gas shift reaction.

High-Pressure Gas Clean-Up Model

Antal et. al. (1996) showed that high pressure water can be used to separate carbon dioxide gas from hydrogen producing a 97% pure hydrogen stream. The process they proposed, shown in Figure 1, was to cool the stream leaving the Supercritical Water Reactor at 38.5 MPa down to 25 °C and mix this cooled stream with a large quantity of pressurized water in a CO_2 absorber, which would produce a gas stream and a liquid stream. The gas stream would be relatively pure hydrogen. The liquid stream would contain most of the CO_2 produced in the reactor along with a significant amount of the hydrogen. By reducing the pressure of the liquid to 0.1 MPa, the dissolved hydrogen and some of the carbon dioxide would be released in a gas-liquid separator. This gas could be used, along with some of the purified hydrogen to heat the incoming biomass slurry up to reactor temperatures. A heat exchanger was also used to heat the incoming biomass slurry up from 25 °C to 440 °C, prior to the heater/combustor.

While the results of their work were promising, Antal's group did not consider the impact of the presence of other gasses that might be present in the stream leaving the reactor. These gases include carbon monoxide, methane and ethane. Since these gases are less soluble in water than carbon dioxide, it is likely that they will further decrease the purity of the hydrogen stream produced by this process. In this task, CSI expanded on the work of Antal's group to examine the effects that methane, ethane and carbon dioxide would have on the proposed separation process.

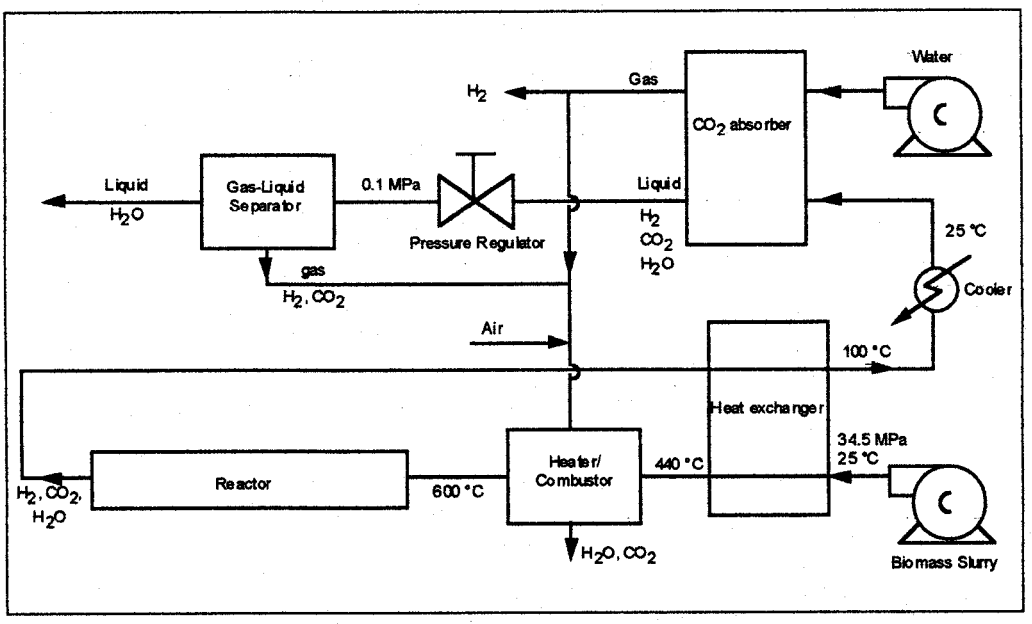

Figure 1 - Biomass gasification process with carbon dioxide separation by adding water. Source: Antal (1996).

The proposed gas clean-up process is shown in Figure 2. All of the calculations shown in this report are related to a proposed 30 g/min. pilot plant. This plant is expected to produce about 0.33 Sm^3/hr of fuel cell grade hydrogen, which contains less than 10 PPM of CO_2. Like the system proposed by Antal (1996), the process utilizes a high-pressure carbon dioxide absorber (HP Absorber) which contacts the cooled reactor products with a large quantity of water. This mixture is then allowed to flash into a gas stream and a liquid stream. The gas stream contains about 98 to 99% of the hydrogen while the liquid stream contains 50 to 70% of the carbon dioxide.

The liquid from the HP Absorber flows through a pressure-reducing valve where the pressure is reduced to atmospheric pressure. At this pressure, a second flash vessel (LP Flash) will produce a water stream that contains a small amount of CO_2 and a vent gas stream that contains mostly CO_2 and water vapor. The carbon dioxide content of the water leaving the second flash vessel is low enough that pressurizing the water and recycling it will not result in a build-up of CO_2.

The producer gas leaving the HP Absorber is enriched in hydrogen. The concentration of hydrogen at this point is about 70% to 80% on a mole basis, depending on the performance of the reactor. This producer gas has a heating value that is suitable for use in a gas turbine, provided the right size of turbine could be found. To further purify the gas stream, thin film palladium-silver membranes are utilized. These membranes operate at 350 °C, therefore the gas has to be heated to this temperature in a gas heater. After passing through one membrane, the gas stream is suitable for use as compressed gas (99.95% pure hydrogen). A second membrane is required to purify the hydrogen product to a level suitable for a fuel cell (greater than 99.99% pure and a CO concentration less than 10 PPM). The waste gas leaving the membranes will be enriched in methane and

CO. This gas can have a heating value in the range of 350 to over 500 Btu/ft^3, depending on the performance of the reactor, and is suitable for use by the process to provide heat to both the reactor and to the gas heater.

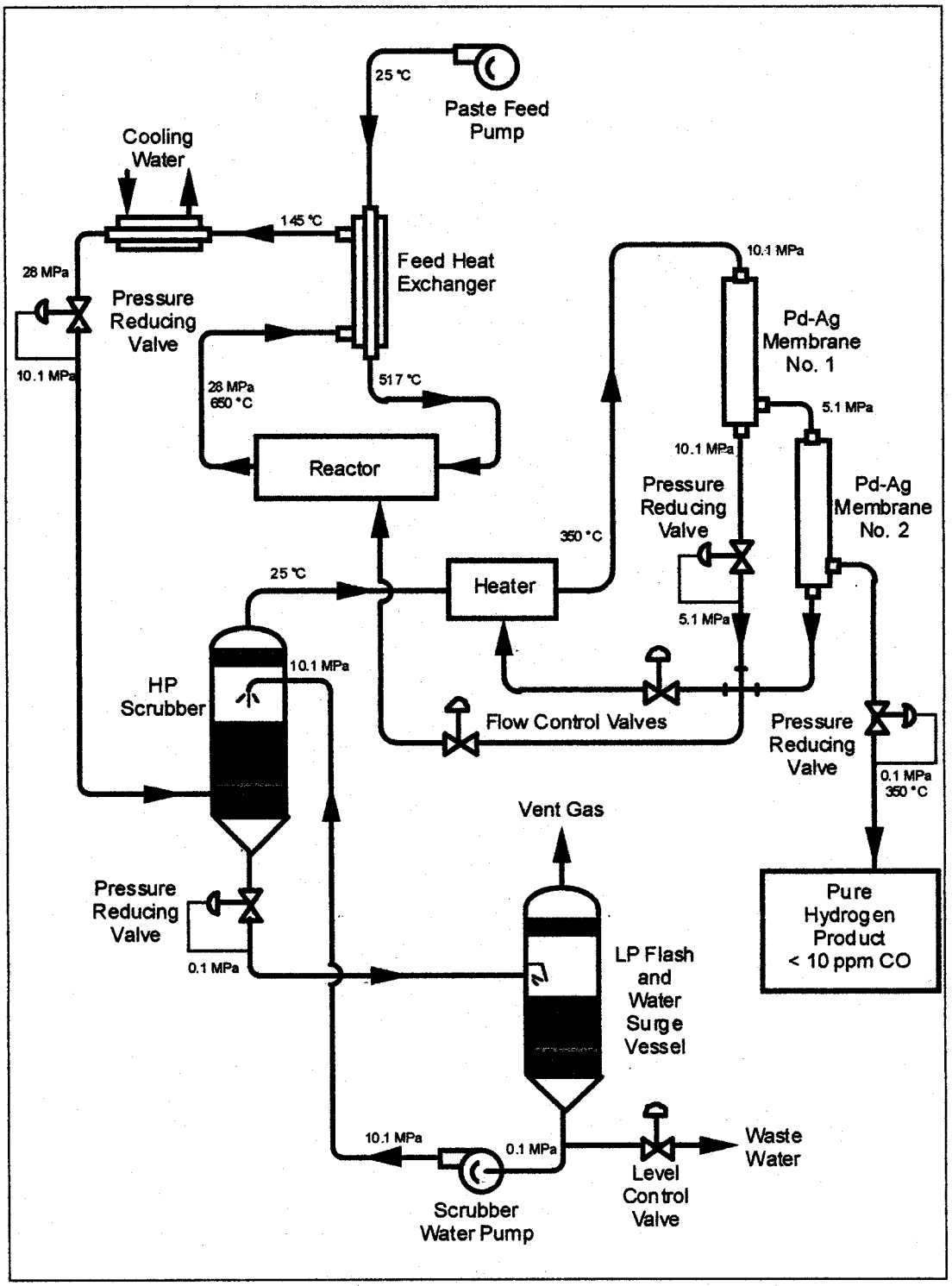

Figure 2 - Schematic of the proposed gas clean-up process.

High Pressure Absorber

The HP Absorber mixes recycled water with the cooled water coming from the reactor. This absorber operates at a pressure anywhere from 10 to 25 MPa. The pressure of the absorber will have an impact on the quantity of hydrogen in the vent gas from the LP Flash vessel. Figure 3 shows the relationship between the operating pressure of the HP absorber and the percent of hydrogen loss via the vent gas. This figure was calculated for a water recirculation ratio of 10.

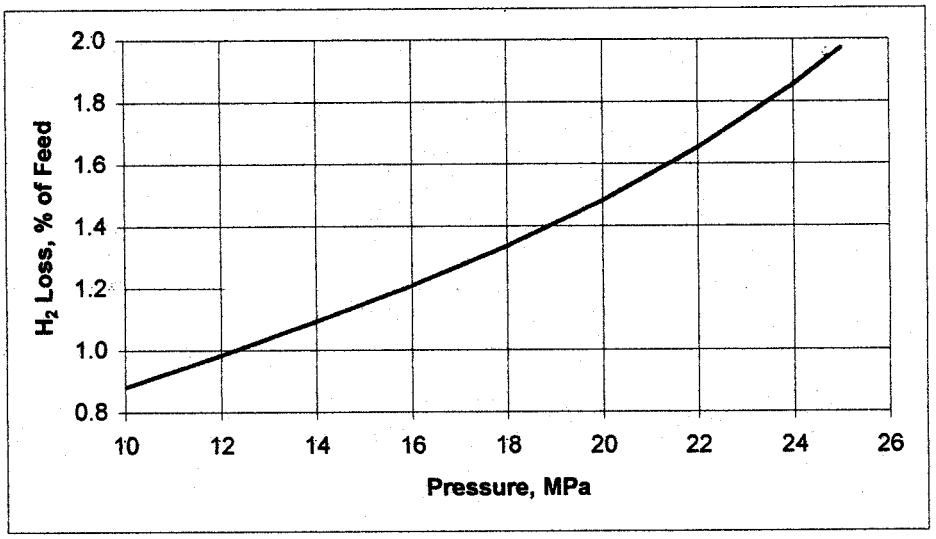

Figure 3 - Effect of HP scrubber vessel pressure on hydrogen loss

Another parameter that impacts the performance of the absorber is the ratio of recycle water to fluid leaving the reactor. Higher water flow rates will absorb more CO_2 in the liquid. This will result in a higher heating value for the Producer gas stream. Figure 4 shows the relationship between the amount of recycle water and the percentage of CO_2 absorption and the heating value of the Producer gas. This figure shows that above recirculation ratios of 20 there is little benefit to the heating value of the gas. While a recycle ratio of 20 sounds large, for the pilot plant that is considered here this recycle rate would translate to about 600 cc/min. (less than 10 GPH).

The producer gas leaving the HP absorber is enriched in hydrogen. Unfortunately, the Henry constants for CO, methane and ethane are all greater than the Henry constant for hydrogen. Therefore, most of these gases leave the HP absorber with the gas stream and contaminate the producer gas product. Figure 5 shows the impact of the water recycle rate on the hydrogen purity leaving the HP absorber. This figure shows that, even at very high water recycle ratios, the purity of hydrogen is limited by the presence of these other gases. Therefore, further gas clean up is required, unless this gas is going to be run through a gas turbine.

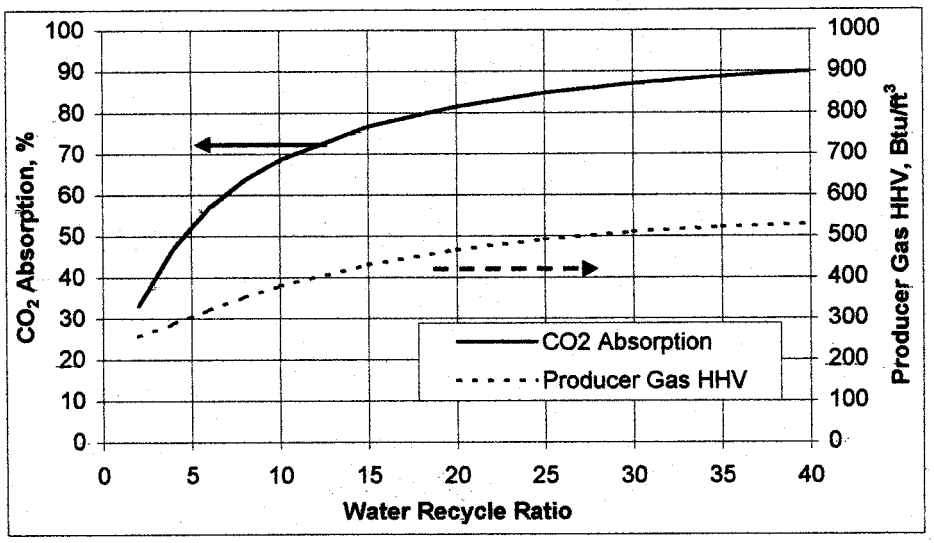

Figure 4 - Effect of recycle on CO_2 absorption and producer gas HHV.

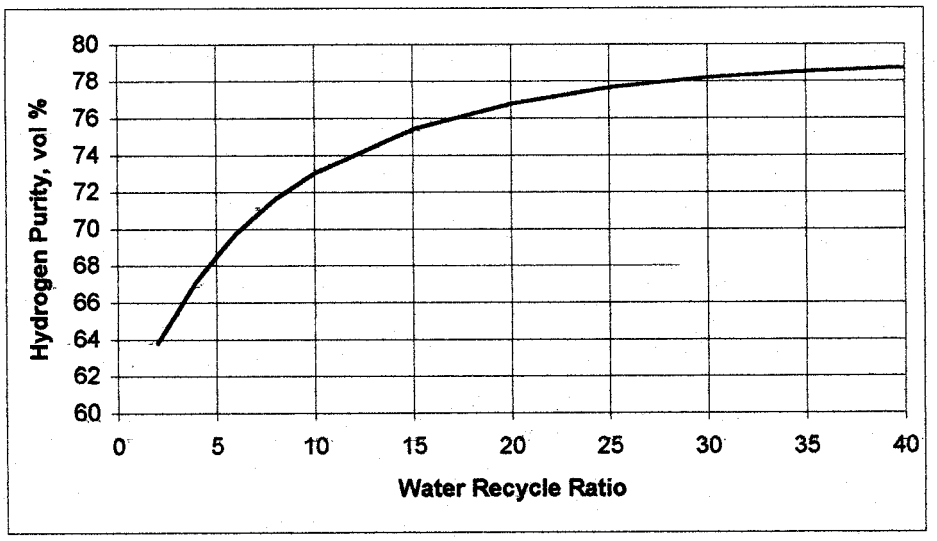

Figure 5 - Effect of recycle ratio on hydrogen purity from the HP scrubber.

Global Model of the SCW Pyrolysis Process

The supercritical water pyrolysis of biomass involves a complex set of chemical reactions among numerous reacting species. A detailed model of this process, which identifies all of the possible reaction pathways, would be impossible to develop at this time. In fact, it is likely that not all of the intermediate reaction compounds have even been identified at this time. In this section, we will develop a global reaction scheme that attempts to identify what we believe to be the major reaction pathways.

Figure 6 shows the proposed global reaction mechanism for the pyrolysis of biomass in supercritical water. A total of 14 reaction pathways are shown in this scheme. Wood decomposes in water at temperatures below the critical point by two parallel reaction pathways. The first is the acid catalyzed formation of tar, which leads to char deposits at the inlet of the reactor. The second wood decomposition reaction fits a first-order reaction rate that leads to intermediate compounds, which are referred to as "Non-Tar" in Figure 3-1. All of the wood is dissolved into tar or non-tar compounds at temperatures below the critical point. It should be pointed out here that the term Non-Tar is used just to differentiate between compounds that are char precursors and those that are not. The non-tar compounds react along six separate parallel primary pathways. The first two, the formation of propenoic acid and acetic acid are acid catalyzed reactions that occur at temperatures below the critical point. The other four are gasification reactions producing hydrogen, carbon dioxide, methane, and carbon monoxide.

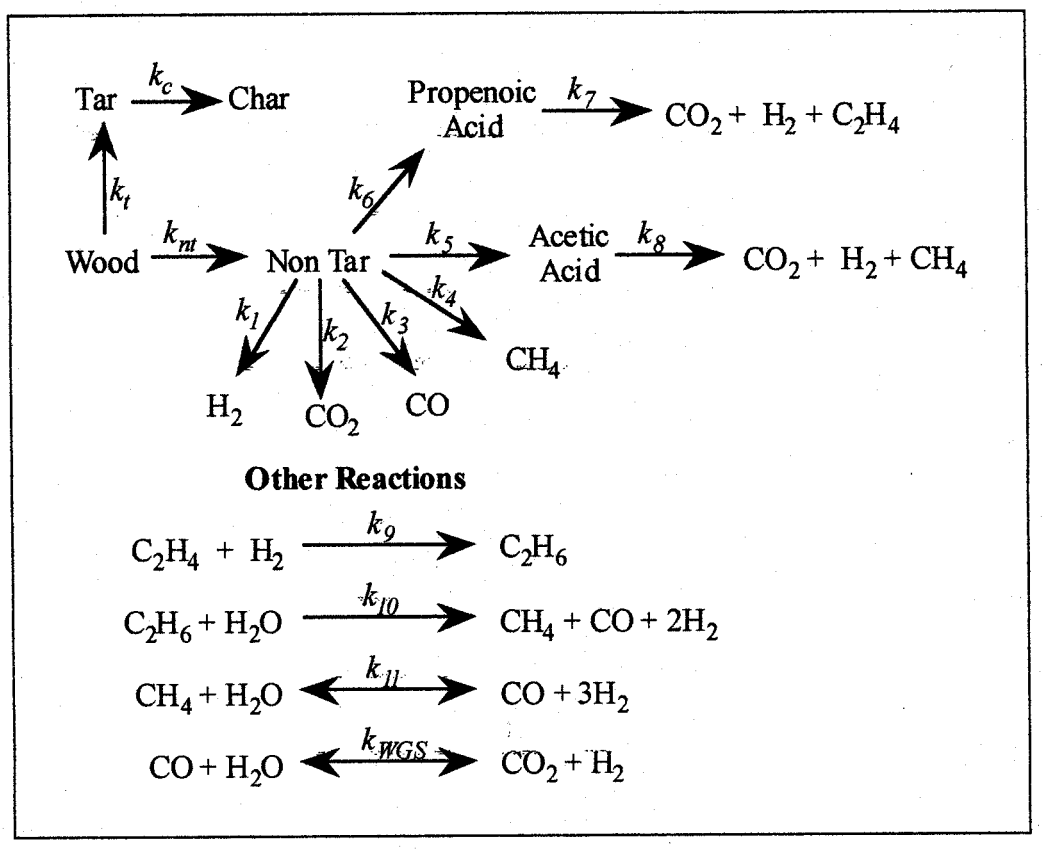

Figure 6 - Proposed global reaction mechanism for SCW Pyrolysis.

Secondary pathways include the destruction of propenoic acid and acetic acid. Propenoic acid decomposes to form ethylene, CO_2 and H_2. Acetic acid decomposes to form methane, CO_2 and H_2. Other reactions that are considered in this mechanism include the hydrogenation of ethylene, the destruction of ethane and methane by water, and the water-gas shift reaction. Ethylene reacts with hydrogen to form ethane, which then reacts

with water to form methane, CO and hydrogen. Methane reacts with water to form CO and hydrogen in a chemically reversible reaction. The water-gas shift reaction is also a chemically reversible reaction, which is assumed to be mass transfer controlled.

Char Formation Pathway

The char formation reaction occurs below the critical temperature and is the result of dehydration and carbon cross linking of hemicellulose and lignin fragments. Between 200 and 370 °C, the dielectric constant and the ionic dissociation constant are such that organic compounds are not soluble in water. Furthermore, at the pressures of these experiments, the ionic dissociation constant, K_W, of the water is in the range of 10^{-11} to 10^{-12} $(mol/kg)^2$. Therefore, the water is capable of promoting an acid catalyzed dehydration reaction of the wood matrix. The acid catalyzed dehydration reactions of the hemicellulose and lignin compounds produce tars, which deposit on the walls of the reactor. Once fixed to the walls, they continue to cross link and eventually form char. The deposit continues to grow in this manner until the reactor entrance is completely plugged.

Figure 6 shows the proposed char formation pathway in the upper left-hand corner. The mechanism assumes the initial decomposition of wood forms two products, tars and non-tars. The tars diffuse to the walls of the reactor where they adhere and then slowly turn into char. The actual rate of char formation from the tars is not important since once they adhere to the wall of the reactor, they are removed from the flowing stream. Therefore, for this analysis this rate step can be ignored, although the rate of deposition must be considered.

The rate of disappearance of wood is given by:

$$\frac{\partial[W]}{\partial t} = -\left(k_{nt} + k_t[H^+]\right)[W] \quad \text{, g/L-s} \tag{1}$$

Where: k_{nt} = first order rate constant for the formation of non tar products, 1/s
k_t = first order rate constant for the formation of tars, 1/s
$[H^+]$ = the hydrogen ion concentration from the dissociation of water, g/L
$[W]$ = the concentration of wood, g/L

A simple mass transfer model is assumed for the deposition of tar on the walls of the reactor, where the rate of deposition is proportional to the concentration of the tar in solution. Therefore, the expression that describes the concentration of tar in the water is given by:

$$\frac{\partial[T]}{\partial t} = k_t[H^+][W] - \frac{k_m}{a}[T] \quad \text{, g/L-s} \tag{2}$$

Where: k_m = mass transfer coefficient, m^2/s
a = cross section area for flow, m^2
$[T]$ = concentration of tar in solution, g/L

Finally, the rate of char deposition, D in g/s, on the walls of the reactor is then given by the following expression:

$$D = 1000\int_0^x Y_c k_m [T]dx \quad , g/s \tag{3}$$

Where: Y_c = yield of char, g char/g wood
x = distance, m

The constant 1000 in Equation 3 is needed to convert the units on the concentration from liters to m^3. The value of Y_c is assumed to be the fixed carbon concentration, which is 49.4% for Poplar wood.

Physical descriptions of the char plug indicate that the plug forms in the region of the entrance heater. The plug itself is approximately 1 inch long, and obstructs enough of the flow area to force the pump pressure to rise from 277 bar (4000 psi) to about 346 bar (5000 psi). Based on this limited amount of information, we estimate that a char plug weighing 0.37 g would be sufficient to increase the pump pressure to this point.

During a test on October 29, 1997, the University of Hawaii's supercritical water reactor was operated for about 1 hour and 25 minutes before the reactor plugged. Figure 7 shows the calculated temperature profile inside the University of Hawaii's reactor for the approximate conditions of this test (Divilio 1998). During this test, the concentration of Poplar wood in the feed stream was 11.35% by weight. Based on the above assumption of a char plug weighing 0.37 g, the average char deposition rate, given by Equation 3 would be 7.25×10^{-5} g/s. This information gives us a reference point with which to determine the kinetic rate constant k_t and the mass transfer rate, k_m.

For the first order rate constant for the formation of the non-tar products, we chose to use the kinetic rate expression for the disappearance of glucose that was derived from our literature review (Divilio 1998a). This fit of the glucose data yielded the following rate constant:

$$k_{nt} = 10^{12.325} e^{\frac{-143.2}{RT}} \quad , 1/s \tag{4}$$

where the activation energy is given in kJ/mol. This activation energy of 143.2 kJ/mol is consistent with Bobleter's (1994) estimates for the acid hydrolysis of hemicellulose (106 to 160 kJ/mol) and is also reasonably close to Schwald's (1989) estimate for the activation energy for cellulose hydrolysis (129.1 kJ/mol). We also assumed an activation energy for k_t of 80 kJ/mol, based on Sarakanen's (1981) estimate of the activation energy for the α-aryl ether hydrolysis of lignin.

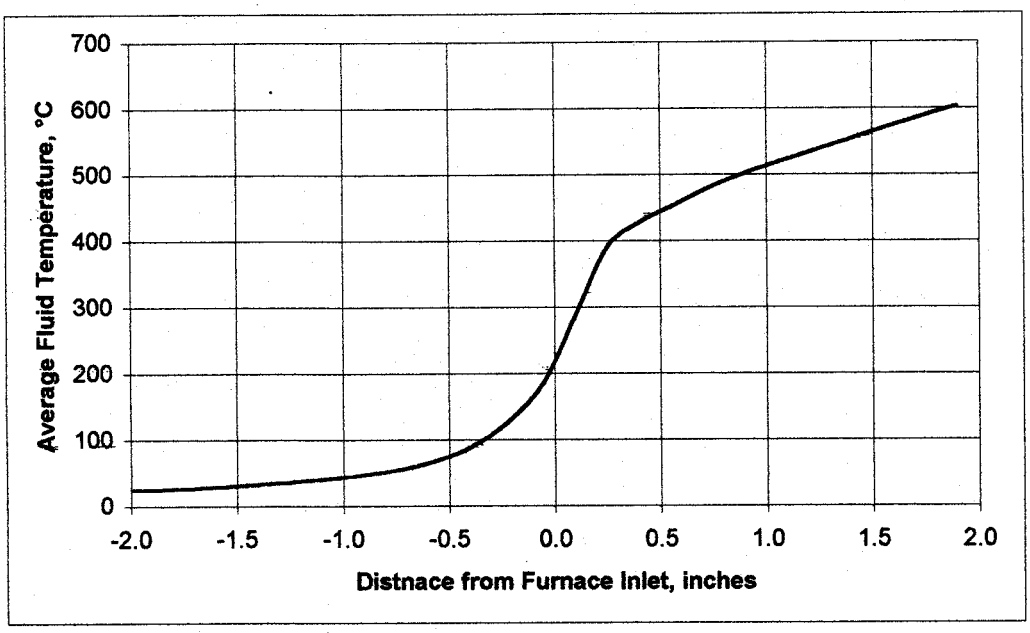

Figure 7 - Calculated temperature profile at the entrance of the University of Hawaii's reactor.

With these assumptions, the only other constants required to solve Equations 1 through 3 are the frequency factor for k_t and the mass transfer coefficient, k_m. To fit these two constants, we first adjusted the mass transfer coefficient such that all of the tar had deposited on the tube walls by the time the fluid had traveled one inch past the start of the entrance heater. We then adjusted the frequency factor for k_t until the integrated deposit rate equaled 7.25 x 10^{-5} g/s, based on our estimate above. As a result of this calculation, we obtained the following expressions:

$$k_t = 10^{9.288} e^{\frac{-80}{RT}}, \text{ 1/s} \qquad (5)$$

$$k_m = 4.488 \text{ x } 10\text{-}5 \quad , \text{m}^2/\text{s} \qquad (6)$$

Figure 8 shows the concentration profiles for wood and tar in the reactor calculated for this test. Figure 9 shows the calculated deposition rate along the length of the reactor. All distances in Figures 7 through 9 refer to the distance from the upstream edge of the entrance heater blocks. Note that the tar begins to be formed even before the paste reaches the entrance heater. Figures 7 and 8 also show that Equation 4 predicts that the wood will be completely dissolved into smaller compounds before the fluid temperature reaches the critical temperature. Figure 8 shows the approximate shape of the char plug. The plug extends from just about 0.1 inches upstream of the entrance heater block to about 1 inch beyond the start of the entrance heater block, which is consistent with descriptions of the plug.

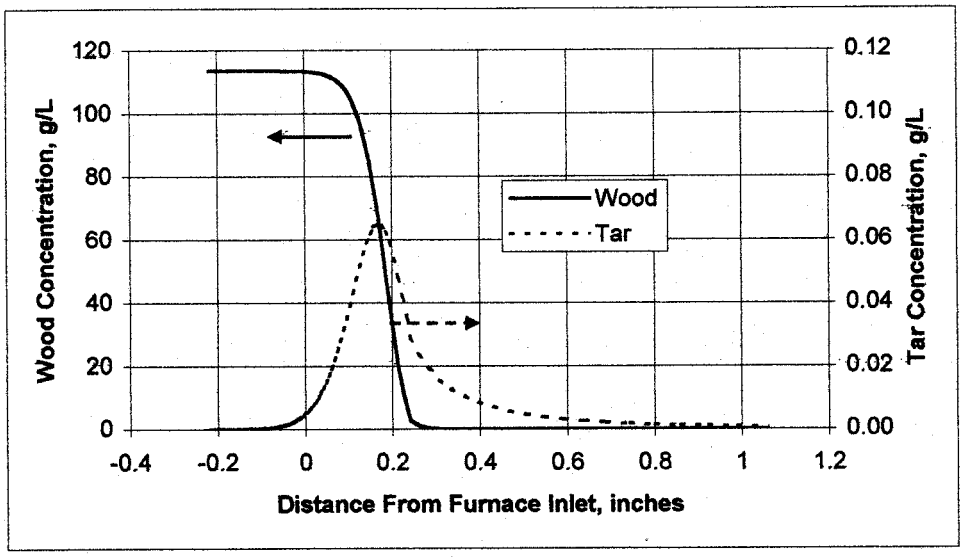

Figure 8 - Wood and tar concentrations v. distance inside the reactor.

To test these values for the reaction rate constants and the mass transfer coefficient, we used data from another test. This test was conducted on May 1, 1997 and utilized a feed stock that contained 5.05 wt. % poplar wood. When Equations 1 through 3 are solved for this wood concentration, keeping all other conditions equal to before, the char deposition rate is calculated to be 3.24×10^{-5} g/s. At this deposition rate, it would have taken 3 hours and 11 minutes for the char plug to grow to a size of 0.37 g. This is consistent with the length of test reported for May 1, 1997. The actual time to the plug formation of the plug is not known, however Antal (1997) reported data for just over 3 hours of on-stream operation.

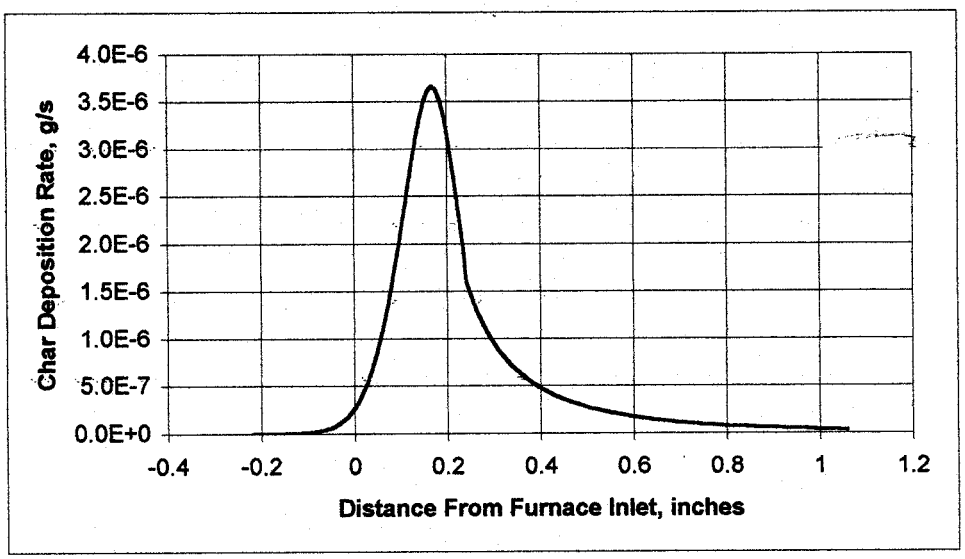

Figure 9 - Char deposition rate v. distance inside the reactor.

Water Gas Shift Reaction

A key reaction in the supercritical water pyrolysis process is the Water-Gas Shift Reaction. The water gas shift reaction is the reaction between carbon monoxide and water to produce hydrogen, and is expressed by the following reaction:

$$CO + H_2O \Leftrightarrow CO_2 + H_2 \qquad (7)$$

Note that the water-gas shift reaction is a reversible chemical reaction. As such, when the product concentrations of CO_2 and H_2 are too high, the rate will reverse and CO_2 and H_2 will react to form CO and water. If left in contact long enough, the four species will achieve equilibrium and the reaction will stop.

Helling, et. al. (1992) measured the reaction rate of the water-gas shift reaction in supercritical water at a pressure of 246 bar and at reaction temperatures ranging from 445 to 593 °C, at residence times of 5.0 to 12.1 seconds. In their analysis of the data, they also modeled the preheat tubing to account for any reaction taking place prior to entering the reactor. This analysis allowed them to calculate the amount of conversion that took place in the preheated tubing, which specifies the concentrations of the reactants and products at essentially isothermal temperatures in the reactor tubing. Their correlation of the kinetic rate took the following form:

$$R_{WGS} = 10^{3.3} Exp\left(-\frac{95}{RT}\right)[CO]^{0.71} \quad \text{, mol/L-s} \qquad (8)$$

Figure 10 shows a comparison of the measured versus the calculated conversions of CO using Equation 8. This figure shows that the rate expression Helling derived does an adequate job of fitting the data. The standard deviation of the calculated results was 2.20%. The thin lines in Figure 8 show the width of one standard deviation.

In spite of the good fit, Helling's rate expression has some serious flaws. First, the expression does not account for the reversible nature of the reaction. In fact, Equation 8 predicts that, given sufficient reaction time, the conversion of CO will go to 100 %. Equilibrium is not a consideration in Helling's work because at the low CO concentrations used, the equilibrium conversion would have been over 99.99%. However, for biomass gasification work, where high hydrogen and low CO concentrations are the objective, the irreversible nature of Equation 8 presents problems.

Secondly, the exponent of 0.71 on the CO concentration indicates that either mass transfer or the reverse reaction is coming into play in the overall mechanism. Yu, et. al. (1993) observed that the yields of hydrogen and CO were dramatically different when different reactor materials were used when conducting pyrolysis experiments with glucose. Inconel and corroded Hastelloy materials showed high hydrogen and low CO yields while a new Hastelloy tube showed much higher CO yields and correspondingly lower hydrogen yields. Based on this observation, Yu concluded that the reactor wall was behaving as a catalyst, possibly for the water-gas shift reaction.

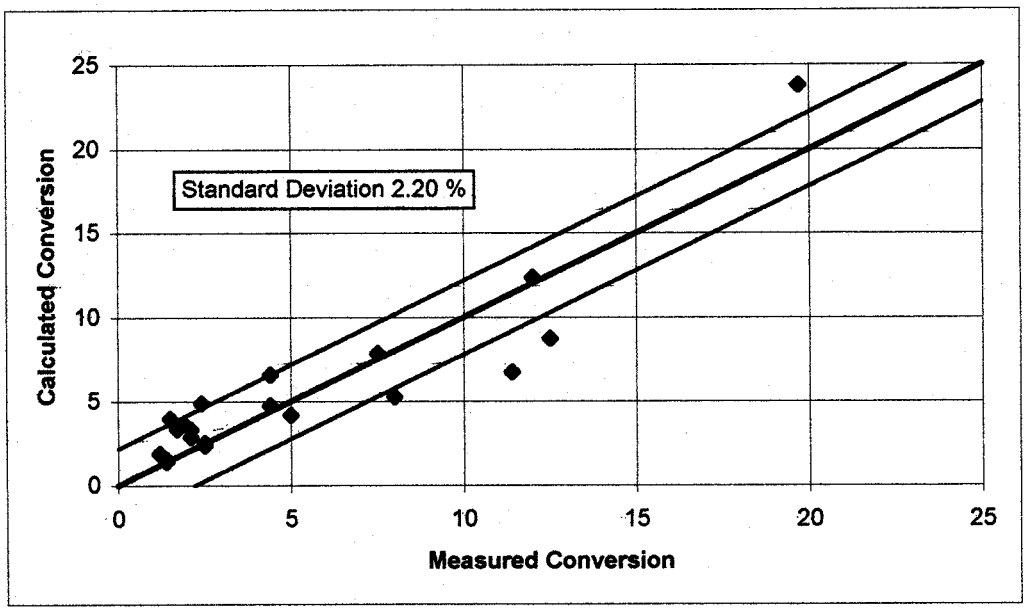

Figure 10. Measured versus calculated CO conversion using Equation 8.

Reversible Kinetic Rate Expression

The first rate expression we tested using Helling's data was a reversible kinetic expression of the form:

$$-\frac{\partial[CO]}{\partial t} = k_{WSG}[CO][H_2O] - k_r[CO_2][H_2] \qquad (9)$$

Where k_{WGS} and k_r are the reaction rate constants for the forward and reverse reaction respectively, in mole/L-sec. At equilibrium, the reaction rate goes to zero and the concentrations of the species are at their equilibrium levels. Thus, k_r is related to k_{WGS} by the following expression:

$$k_r = k_{WGS}\, k_{eq} \qquad (10)$$

Equations 9 and 10 can be used to evaluate the rate constant from Helling's data. For this analysis, the initial concentrations of CO, CO_2 and H_2 were determined from Helling's estimate of the initial conversion of CO entering the isothermal portion of the reactor. This simplified the computational procedure, as the reaction temperature did not vary in the reactor. A regression analysis was performed to determine the values of the activation energy and the frequency factor for k_{WGS} assuming an Arrhenius rate form which best fit the data.

The result of this analysis is shown in Figure 11, which shows the measured conversion of CO, in percent, versus the calculated conversion. The following rate constant was found to fit the data to within a standard deviation of 2.23% conversion:

$$k_{WGS} = 10^{4.82} e^{\left(\frac{-115.25}{RT}\right)} \text{, mol/L-s} \qquad (11)$$

Where the activation energy is in kJ/mol, and T is in °K. Figures 10 and 11 show that Equations 9, 10, and 11 fit the data as well as Helling's expression. In fact, the calculated conversions are nearly identical to those predicted by Helling's rate equation. However, the rate expression given by Equations 9, 10, and 11 will predict the reversible nature of the reaction better than Equation 8. As such, it is a better choice for use in a supercritical water pyrolysis model.

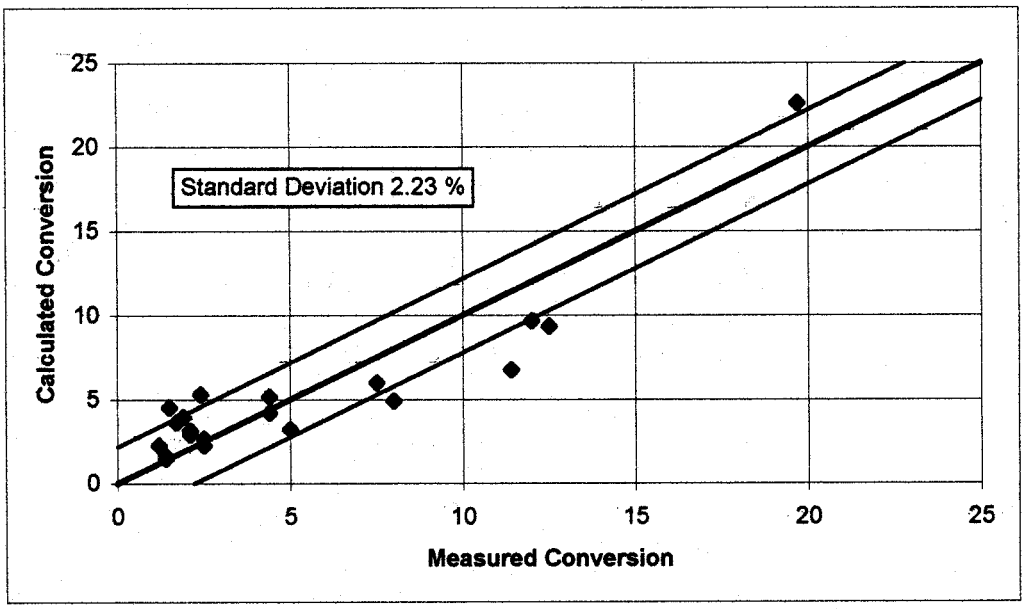

Figure 11 - Measured versus calculated CO conversion using the reversible kinetic rate.

Mass Transfer Model

While the reversible kinetic expression fits the data as well as Helling's expression, it still does not explain Yu's observations of an apparent reactor wall effect. To test if mass transfer is influencing the reaction, a simple mass transfer model was developed. In this model, CO diffuses from the bulk liquid to the surface of the reactor wall, where it reacts to form CO_2 and H_2, which then diffuse back to the bulk liquid. Since the reaction takes place in water, and water is a major reactant, we can ignore the diffusion of water to the reactor wall. The rate of disappearance of CO is then given by the following expression:

$$\frac{d[CO]}{dt} = -\frac{k_m}{a}\left([CO]_b - [CO]_s\right) \qquad (12)$$

Where: k_m = the mass transfer coefficient, m^2/s
a = the cross section flow area, m^2
$[CO]_b$ = the average CO concentration in the bulk fluid, mol/L
$[CO]_s$ = the CO concentration at the wall surface, mol/L

At the surface of the reactor walls, the rate of CO disappearance is given by:

$$\frac{d[CO]}{dt} = k_{WGS}[CO]_s[H_2O] - k_r[CO_2]_s[H_2]_s \tag{13}$$

Since the rate of diffusion of CO to the surface of the wall is equal to the rate of disappearance via the chemical reaction, Equations 12 and 13 can be set equal to each other and solved for the surface CO concentration:

$$[CO]_s = \frac{\frac{k_m}{a}[CO]_b + k_r[CO_2]_s[H_2]_s}{k_{WGS}[H_2O] + \frac{k_m}{a}} \tag{14}$$

Furthermore, if we assume that the rate of mass transfer of CO to the reactor wall is equal to the mass transfer rate of CO_2 away from the reactor wall and is equal to the mass transfer rate of H_2 as well, then the concentrations of CO_2 and H_2 at the surface of the wall will be given by:

$$[CO_2]_s = [CO_2]_b + [CO]_b - [CO]_s \tag{15}$$

and

$$[H_2]_s = [H_2]_b + [CO]_b - [CO]_s \tag{16}$$

Finally for the purpose of this study, we assumed a simple expression for the mass transfer coefficient of the form:

$$k_m = k_{mo}V^n \tag{17}$$

Where V is the velocity of the fluid in the reactor given by the reactor length divided by the residence time in the reactor. Equations 12 through 17 give a system of equations that can be solved to determine the conversion of CO in the bulk fluid. An iterative solution was performed for the surface concentration of CO at every step of the integration. Equation 14 was used to calculate an approximate surface concentration of CO, by assuming that the surface concentrations of H_2 and CO_2 were zero. This value was used to calculate the surface concentrations of CO_2 and H_2 from Equations 15 and 16, and these values were used to calculate a new surface concentration of CO using Equation 14. The process was repeated until the surface concentration of CO converged, at which point, Equation 12 was used to calculate the rate of disappearance of CO from

the fluid. A modified Adams-Moluton method was used to integrate Equation 12. For the regression analysis, values of the activation energy and the frequency factor as well as k_{mo} and n were varied to find the best fit to the data.

The results of the regression analysis are shown in Figure 12. The standard deviation for this fit was 1.33, which is substantially better than the fits obtained by Helling or by the reversible kinetic expression. The standard deviation was adjusted for the two fewer degrees of freedom, which resulted from the use of k_{mo} and n in the data fit. Since a total of 20 data points were fit, the loss of two additional degrees of freedom had only a minor impact on the standard deviation.

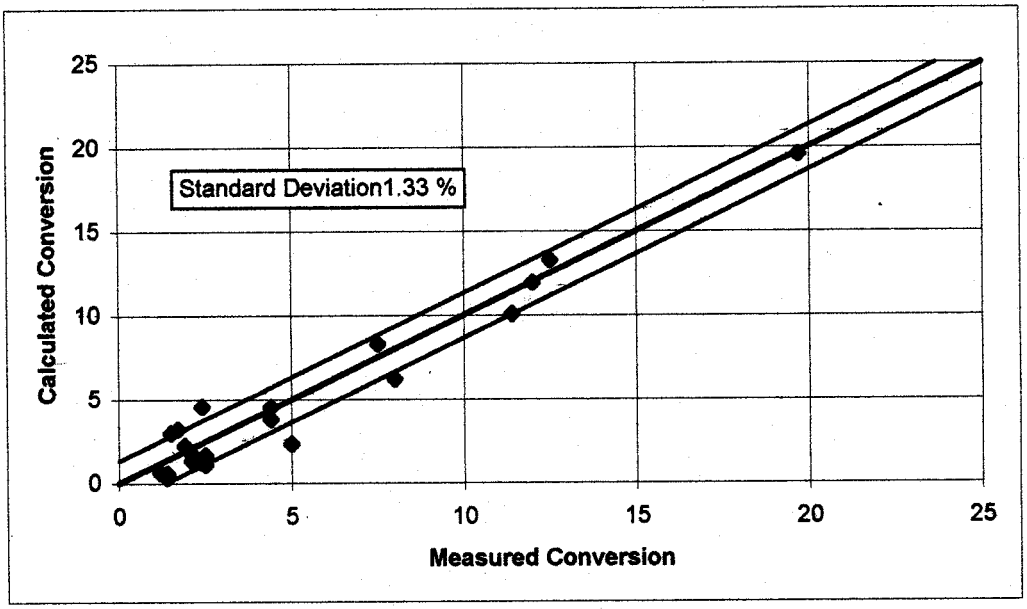

Figure 12 - Measured versus calculated CO conversions using the mass transfer model.

The kinetic rate constant and the mass transfer coefficient were found by the regression analysis to be:

$$k_{WGS} = 10^{15.78} e^{\left(\frac{-276.97}{RT}\right)} \text{, mol/L-s} \qquad (18)$$

$$k_m = 1.21x10^{-7} V^{0.64} \text{, m}^2\text{/s} \qquad (19)$$

Discussion of Results

The above analysis indicates that mass transfer to the reactor wall and rapid reaction at the reactor wall may be an important mechanism in the water-gas shift reaction in supercritical water pyrolysis. Holgate, et. al. (1995) indicated the observation of "an accelerated water-gas" mechanism which is evident at temperatures above 550 °C during the pyrolysis of glucose in supercritical water. The apparatus used by Holgate, et. al. (1995) was essentially the same apparatus used by Helling, et. al. (1992).

Figure 13 shows a comparison of the three initial kinetic reaction rates discussed in this section as a function of temperature. The initial reaction rate assumes a CO concentration of 0.002 mole/L and no CO_2 or H_2 present in the water. Thus, these rates are similar to the rates that would be found at the entrance of the reactor in some of Helling's tests. The rate indicated as "Mass Transfer Rate" is the surface kinetic rate calculated assuming a surface concentration of 0.002 mol/L and was calculated using Equation 13. Figure 13 shows that the initial rate for Helling's correlation (Equation 8) and the Reversible Kinetic Rate expression (Equation 9) were nearly identical. However, the surface reaction rate exceeds the simple kinetic rates at temperatures above 500 °C. Below 500 °C, all three rates are quite slow.

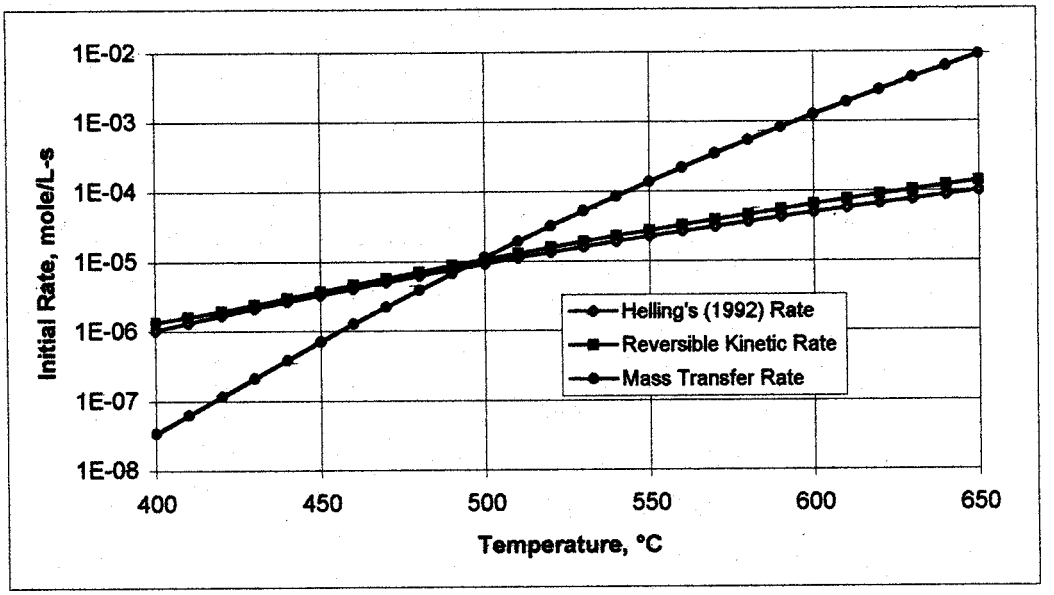

Figure 13. Comparison of Initial Water-Gas Shift reaction rates. Initial rates assume CO concentrations of 0.002 mol/L.

Figure 13 could explain the fast water-gas shift mechanism observed by Holgate, et. al. (1995). If the pyrolysis reactions that produce CO are occurring at or near the tube surface, the mass transfer model predicts that the water-gas shift reaction rate would appear to be occurring much faster than predicted by either Equation 8 or 9. At 550 °C,

the surface reaction rate would be almost 5 times faster than the rates predicted by the kinetic models.

The mass transfer model would also explain Yu's (1993) observations regarding the tube material. It is likely that the Hastelloy and the Inconel materials have different rate constants for the surface reaction due to their compositional differences. Corroded Hastelloy would have more surface area available for the reaction to occur, which would tend to offset the lower kinetic rate.

Another indication of the validity of the mass transfer approach is given by Helling, et. al. (1992). They performed a similar analysis of some of their previous water gas shift experiments (Helling and Tester 1987) that were conducted in a different apparatus. Their rate equation for the previous data was fit by the following expression:

$$R_{WGS} = 10^{2.6} Exp\left(-\frac{67}{RT}\right)[CO]^{0.81} \qquad \text{mol/L-s} \qquad (20)$$

The older apparatus had a 0.211-cm inside diameter while the newer apparatus had a 0.171-cm inside diameter. Helling was unable to explain the reason for the different rate expressions between the two reactor configurations, or for the fact that the older data exhibited a higher apparent reaction rate. Equation 20 predicts an initial reaction rate that is an order of magnitude greater than the initial rate calculated using Equation 8. It should be pointed out that if all conditions are kept the same, the current mass transfer model predicts that the conversion with the older apparatus would be slightly lower than the CO conversion with the newer apparatus. However, this does not take into account changes in velocity, which would also impact the mass transfer rate. Unfortunately, the data from Helling and Tester's (1987) previous experiments were not presented in sufficient detail to analyze using the current mass transfer model.

Glucose Model

Because there was insufficient data to evaluate the global model, shown in Figure 6, we were forced to develop a global model for the SCW pyrolysis of glucose. Figure 14 shows the reaction pathways for the Glucose model. This model is similar to the one shown in Figure 6, with the exception of the char formation pathway, which has been eliminated. A full derivation of the glucose model is beyond the scope of this paper. Instead, we refer the interested reader to Divilio (1998a).

To fit this model, we chose the glucose pyrolysis data of Holgate (1995). Their data contains information on the pyrolysis products between 425 and 600 °C, including data on propenoic acid and acetic acid. As such this data can provide insights into the mechanisms that are not possible from the University of Hawaii's wood paste data. To fit the necessary coefficients for the reactions, a regression analysis was performed on Holgate's data. Figures 15, 16, and 17 show the results of this analysis. For details of the regression analysis see (Divilio 1998a).

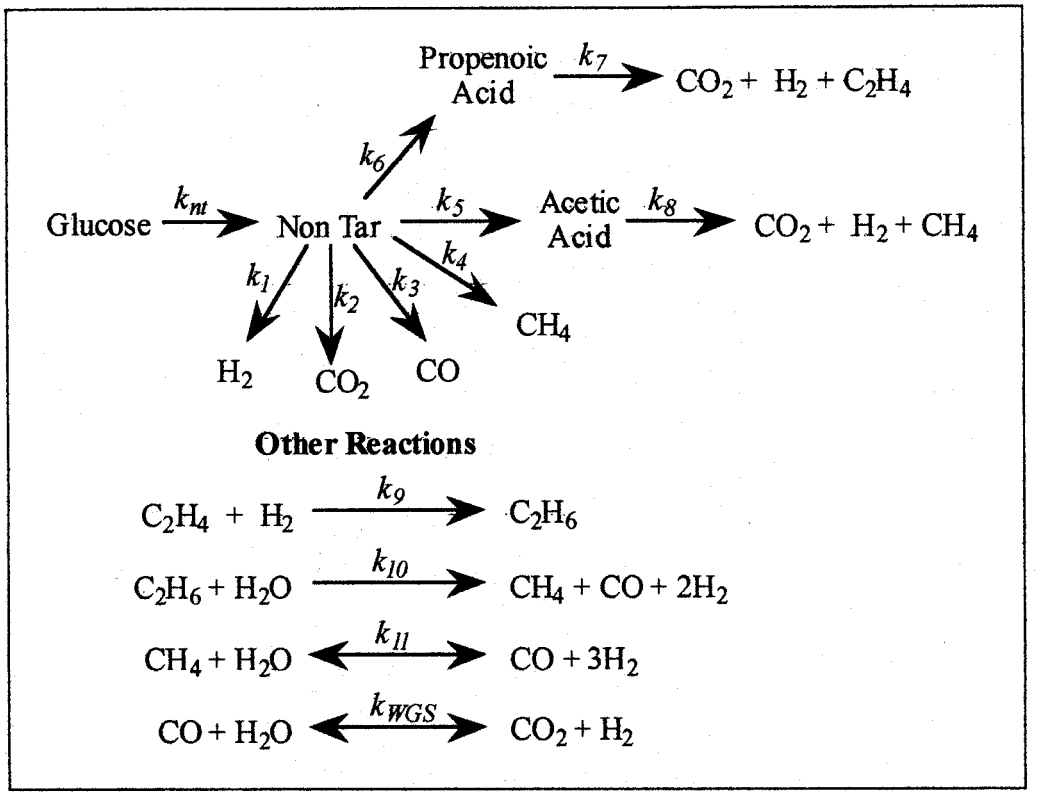

Figure 14. Proposed Glucose model.

Figure 15 shows a comparison of the measured versus calculated concentrations, in mol/mol glucose, for H_2, CO_2 and CO. Figure 16 shows a comparison of the measured versus calculated concentrations of CO, acetic acid and methane. Figure 17 shows a comparison of the measured versus calculated concentrations of ethane, ethylene and propenoic acid. These figures show that the coefficients found do a good job of fitting the data.

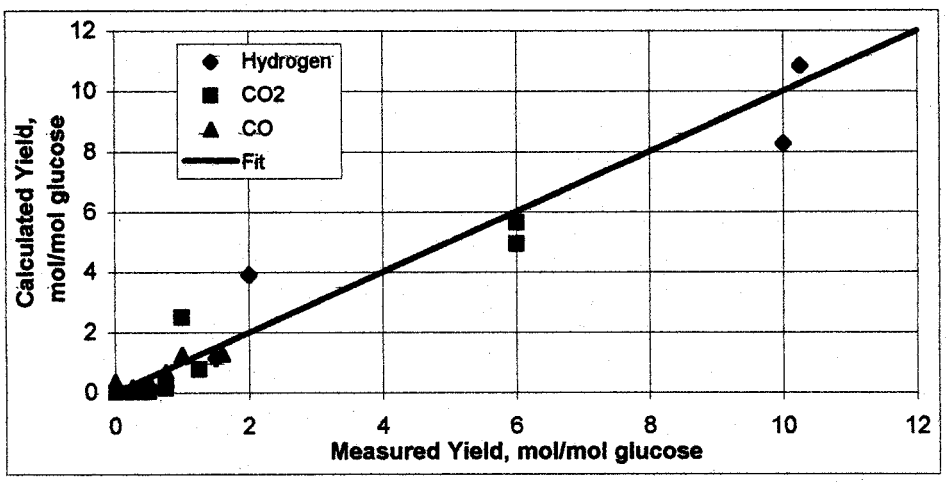

Figure 15 - Measured v. calculated yields of H_2, CO_2, and CO.

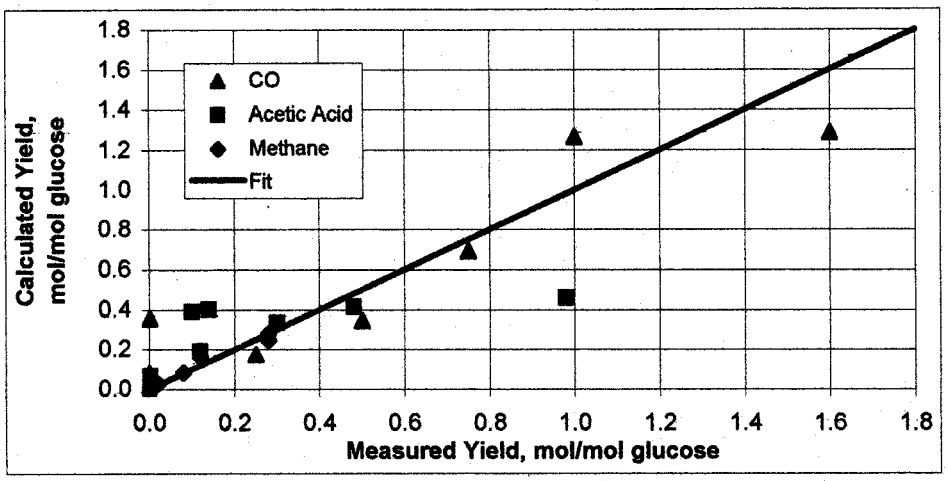

Figure 16 - Measured v. calculated yields of CO, Acetic Acid and CH_4.

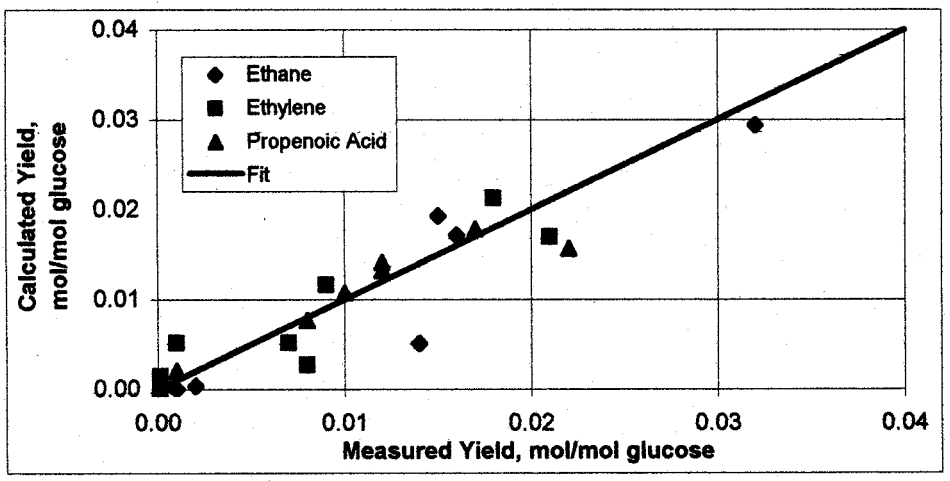

Figure 17 - Measured v. calculated yields of C_2H_6, C_2H_4, and propenoic acid.

Yield Predictions

The results of the regression analysis can be used to show the concentrations of the various species as a function of time in the heater and reactor. Figure 18 shows the yield profile for the pyrolysis of 0.001 M glucose at a reactor temperature of 600 °C. The concentrations of glucose, Non-Tar, acetic acid and CO are shown on the left-hand axis of the upper graph in Figure 18 and the concentrations of H_2, CO_2 and methane are shown on the right-hand axis. The lower graph in Figure 18 shows the yield of ethylene and ethane on the left-hand axis and hydrogen on the right-hand axis. At 600 °C, hydrogen and CO_2 are the major reaction products. Glucose completely disappears by about 6 seconds. At this point in Holgate's reactor, the fluid has just reached the temperature of about 375 °C, and is still in the preheater tube. Hydrogen and CO_2 begin

to evolve at about 8.5 seconds. In Holgate's apparatus, this is still in the heater tube that precedes their reactor. At this point, the fluid temperature is already above 550 °C. This shows the importance of considering the time temperature profile when evaluating the pyrolysis data.

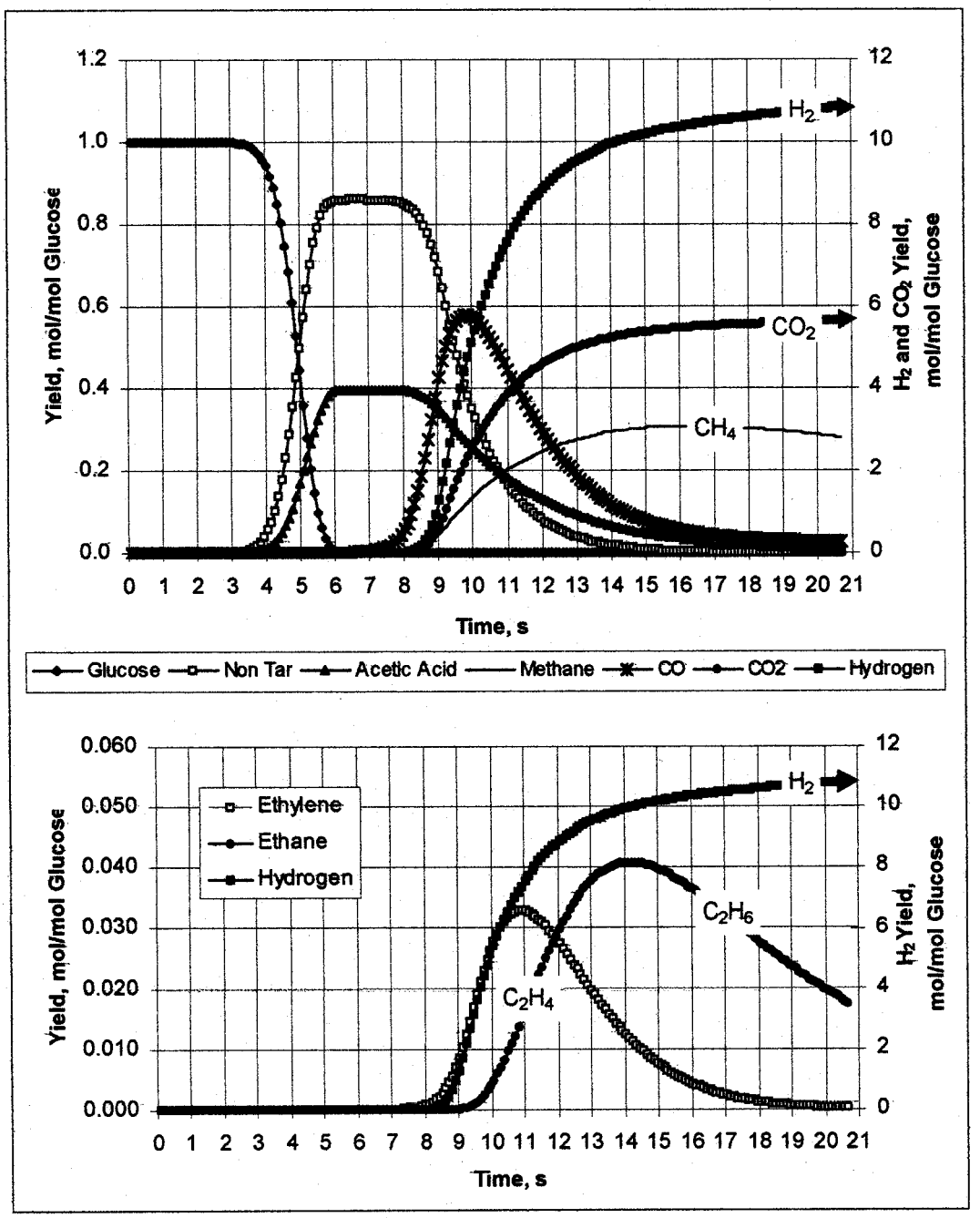

Figure 18. Predicted yield profiles at 600 °C for 0.001 M glucose.

Effect of Heating Rate

Figures 19 and 20 show the effect of the heating rate on the pyrolysis reactions. In both of these hypothetical tests, the time that the reactants spent in the reactor at 600 °C was 10 seconds. However, in Figure 19, the reactants were heated up to 600 °C in only 10 seconds (Fast heating rate), while in Figure 20, the reactants were heated up to 600 °C in 40 seconds (Slow heating rate).

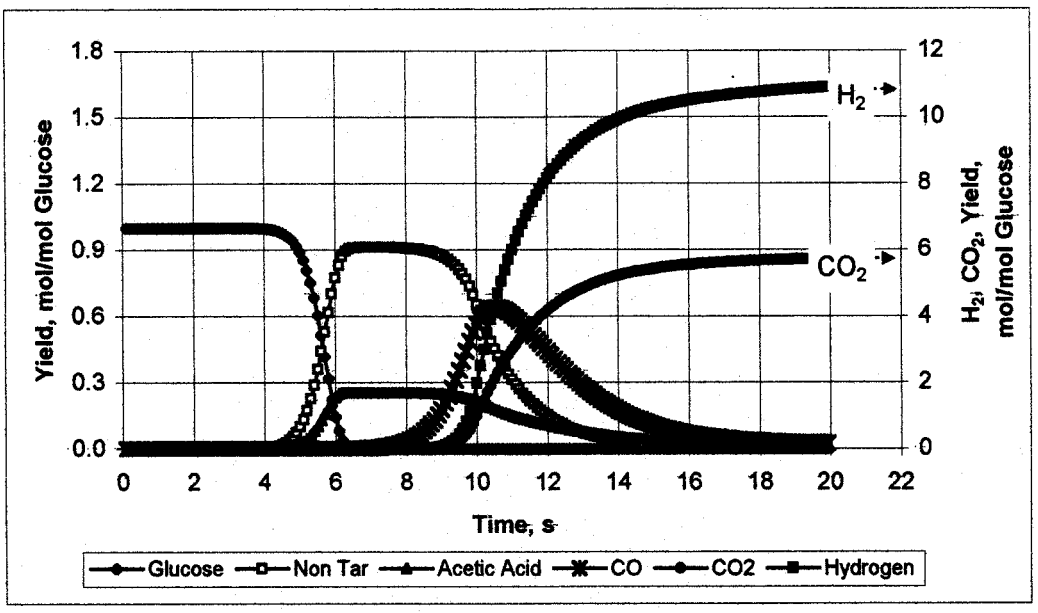

Figure 19. Yield profiles for a fast heating rate for 0.001 M glucose with 10 seconds at 600 °C.

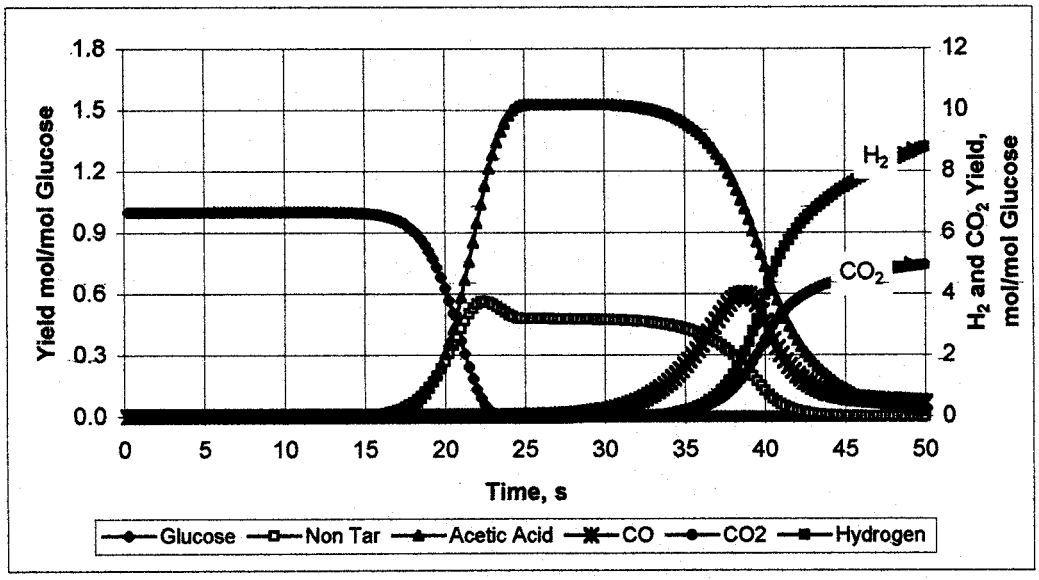

Figure 20. Yield profiles for a slow heating rate for 0.001 M glucose with 10 seconds at 600 °C.

These two figures show that the slow heating rate prolongs the time that the reactants spend in the critical temperature range of 200 to 400 °C. In this temperature range, acetic acid is produced, which has been found by Xu, et. al. (1996) to be highly refractory under SCW Pyrolysis conditions. The glucose model also showed that increased reactor residence time would compensate for the effects of longer heat-up rates.

The effect of the heating rate is important when evaluating data from a test apparatus. The reason for this is that the reactor usually has a fixed length. Therefore, anything that decreases the heating rate will result in less time that the reactants spend at test temperatures. The shortened time at reactor temperatures combined with the increased generation of acetic acid would have a significant impact on the hydrogen yield.

Conclusions

In this paper, we presented a gas clean-up process for the reaction products from the University of Hawaii's Supercritical Water Pyrolysis Process. This gas clean-up process takes advantage of the fact that the products are produced at high pressures (28 MPa) and also takes advantage of the selective solubility of carbon dioxide in water at high pressures to yield a producer gas that is suitable for use in a small gas turbine without further processing. Thin Palladium-Silver membranes are used to further purify the producer gas. After passing through one membrane, the resulting hydrogen gas is cylinder grade (99.95% pure Hydrogen). After passing this hydrogen stream through a second membrane, the resulting gas will be suitable for use in a PEM fuel cell (greater than 99.99% pure and a CO concentration less than 10 ppm).

This gas clean-up process is extremely energy efficient because, unlike other hydrogen gas clean-up processes, no gas compression is required. Only incompressible liquids (water and the wood paste) are pressurized in this design. The Pd-Ag membranes do require that the gases be heated to 350 °C. However, by the time they are heated, the gas volume is relatively small, and waste heat from the reactor can be utilized to provide this heat.

While developing a global model of the SCW pyrolysis process, we developed a model to explain the formation of char at the entrance of the University of Hawaii's Reactor. This mechanism assumes that tar products evolve due to acid catalyzed reactions at temperatures below the critical point of water and that these tar products deposit on the reactor walls and continue to undergo cross linking reactions resulting in the char plug. The model predicts that these tar compounds are formed in the first 1 cm (0.4 inches) from the entrance the reactor (defined as the beginning of the entrance heater) and that the maximum rate of evolution occurs at approximately 0.45 cm (0.18 inches) into the reactor. The model also predicts that the wood completely dissolves into solution in this same region of the reactor. Furthermore, the model successfully predicts the impact of wood concentration in the feed stock on the growth rate of the char plug.

In developing the preliminary model, we performed an analysis of the data of Helling, et. al. (1992) for the water-gas shift reaction. We developed a reversible rate expression that also accounts for mass transfer of CO to the reactor wall. This mechanism significantly improved the fit of the data. The activation energy for the forward reaction was found to be 276.97 kJ/mol, which is significantly higher than the value of 95 kJ/mol reported by Helling. This model also partly explains the "Fast Water-Gas Shift" reaction pathway that was observed by both Holgate, et. al. (1995) and Xu, et. al. (1996).

The preliminary glucose model was calibrated using data from Holgate, et. al. (1995) for the pyrolysis of 0.001 M glucose in supercritical water at temperatures up to 600 °C. This model was found to do a reasonable job of fitting Holgate's data and allowed us to look at the effect of different heating rates on the gaseous products. The model predicted that slower heating rates would decrease the hydrogen yield by as much as 25% when the heating section took 40 seconds to heat the reactants to 600 °C as compared to the hydrogen yield at a heating rate which required only 10 seconds to raise the reactants to 600 °C. However, the model also predicted that increased residence time in the reactor at reactor temperatures would compensate for the decreased hydrogen yield. The first of these predictions has been observed in data at the University of Hawaii (Divilio 1998). However, the second prediction has yet to be tested.

Acknowledgments

This work was funded by the Department of Energy and the National Renewable Energy Laboratory (AXE-8-17103-01). We are particularly grateful to Dr. Michael Antal, Jr. of the University of Hawaii for allowing us to use his data and for his assistance on this project.

References

Antal, M. J. Jr., and X. Xu, 1997, "Total Catalytic Supercritical Steam Reforming of Biomass", Annual Report for Coop. Agreement DE-FG36-94AL85804.

Bobleter, O, 1994, "Hydrothermal Degradation of Polymers Derived From Plants", *Prog. Polym. Sci.*, Vol. 19, p797-841.

Divilio R. J., 1998, "Modeling of Biomass to Hydrogen via the Supercritical Water Pyrolysis Process", Proceedings of the 1988 US DOE Hydrogen Program Review, April 28-30, 1998, Alexandria, VA, p655

Divilio, R. J., 1988a, "Global Model for the Supercritical Water Pyrolysis of Biomass", Activity 2 Report to NREL, November 23, 1998.

Helling, R. K., and Tester, J. W., 1987, "Oxidation Kinetics of Carbon Monoxide in Supercritical Water", *Energy & Fuels*, *1*, p 417.

Helling , R. K., R. H. Holgate, P. A. Webley, and J. W. Tester, 1992, "Carbon Monoxide Oxidation in Supercritical Water: The Effects of Heat Transfer and the Water-Gas Shift Reaction on Observed Kinetics", *Energy & Fuels*, *6*, p 586.

Holgate, H. R., J. C. Meyer, and J. W. Tester, 1995, "Glucose Hydrolysis and Oxidation in Supercritical Water", *AIChE Journal*, Vol. 41, No. 3, March, 1995, p 637.

Sarakanen, K. V. and L. H. Hoo, 1981, *J. Wood Chem. Technol.*, *1*, p11.

Schwald, W. and O. Bobleter, 1989, *J. Carbohydrate Chem.*, *8*, p565.

Xu, X., Y. Matsumura, J. Stenberg, and M. J. Antal Jr., 1996, "Carbon Catalyzed Gasification of Organic Feedstocks in Supercritical Water", *Ind. Eng. Chem. Res.*, Vol. 35, No 8, p2522

Yu, D., M. Aihara, and M. J. Antal, Jr., 1993, "Hydrogen Production by Steam Reforming Glucose in Supercritical Water", *Energy & Fuels*, *7*, p 574.